Available online at www.sciencedirect.com

ScienceDirect

Journal of the European Ceramic Society 35 (2015) 711–721

www.elsevier.com/locate/jeurceramsoc

Waste-to-resource preparation of a porous ceramic membrane support featuring elongated mullite whiskers with enhanced porosity and permeance

Li Zhu [a,b], Yingchao Dong [a,b,*], Stuart Hampshire [c], Sophie Cerneaux [d], Louis Winnubst [e]

[a] CAS Key Laboratory of Urban Pollutant Conversion, Institute of Urban Environment, Chinese Academy of Sciences, PR China
[b] Ningbo Urban Environment Observation and Research Station—NUEORS, Chinese Academy of Sciences, PR China
[c] Materials and Surface Science Institute (MSSI), University of Limerick (UL), Limerick, Ireland
[d] Institut Europeen des Membranes, UMR 5635, Place Eugene Bataillon, 34095 Montpellier Cedex 5, France
[e] Inorganic Membranes, MESA+ Institute for Nanotechnology, University of Twente, PO Box 217, 7500AE Enschede, The Netherlands

Received 16 June 2014; received in revised form 1 September 2014; accepted 9 September 2014
Available online 1 October 2014

Abstract

Different from traditional particle packing structure, a porous structure of ceramic membrane support was fabricated, featuring elongated mullite whiskers with enhanced porosity, permeance and sufficient mechanical strength. The effect of additives (MoO_3 and AlF_3) and sintering procedure on open porosity, mechanical properties, pore size distribution, micro-structure, phase structure, and permeance of the membrane supports was characterized in detail. The introduction of MoO_3 and AlF_3 promoted formation of a porous whisker-interlocked structure, which effectively improved open porosity and permeance. A mullite membrane support containing 5 wt.% MoO_3 and 4 wt.% AlF_3 exhibited an open porosity as high as $48.6 \pm 0.5\%$, a mechanical strength of 81.2 ± 3.2 MPa at 1200 °C, and the value of permeance was higher than the membrane without any additives. Such enhancements in porosity and permeance, with sufficient mechanical strength, were a result of tortuosity decrease due to a porous structure of interlocked mullite whiskers.

Keywords: Ceramic membrane support; Porosity; Mechanical strength; Mullite whiskers; Permeance

1. Introduction

Porous ceramic separation membranes are used in industrial fields due to their unique advantages, such as excellent temperature stability, good pressure resistance, good chemical stability, long life and good antifouling properties.[1] However, commercial porous ceramic membranes still cannot fulfill increasing environmental requirements at a large scale such as separation in strong alkaline media and massive liquid waste treatment due to the limited types of membrane materials[2] (such as Al_2O_3, ZrO_2, SiO_2, TiO_2 and their composites). Besides, high cost, associated with starting materials and formation/sintering processes, makes extensive applications of ceramic membranes still limited.[3,4] As a result, the preparation and potential applications of porous mineral-based ceramic membranes (kaolin,[5] bauxite,[6] sepiolite clay,[7] industrial solid waste coal fly ash,[8] etc) have attracted more attention due to the low cost of abundant raw materials available worldwide. For example coal fly ash emerges as a by-product from the combustion of raw coal in thermal power plants.[9] Without suitable treatment, fly ash may be a source of dust which adversely affects our environment. Therefore, it is necessary to utilize this waste not only to decrease environmental pollution but to produce high added-value products from it. Especially fly ash containing Al_2O_3 and SiO_2 is suitable for the fabrication of dense mullite-based ceramics, as has been proven in.[10,11] Recently a study has been made on the conversion of coal fly ash to mullite ($3Al_2O_3{\cdot}2SiO_2$) for the preparation porous ceramic membranes.[12]

As a structural material, porous mineral-based mullite is expected to be a promising candidate for ceramic membrane supports especially because of its excellent high temperature resistance, good corrosion resistance, abundant natural Al and

* Corresponding author at: CAS Key Laboratory of Urban Pollutant Conversion, Institute of Urban Environment, Chinese Academy of Sciences, Xiamen, PR China. Tel.: +86 0592 6190790; fax: +86 0592 6190790.
E-mail addresses: ycdong@iue.ac.cn, dongyc9@mail.ustc.edu.cn (Y. Dong).

http://dx.doi.org/10.1016/j.jeurceramsoc.2014.09.016
0955-2219/

Si-sources, low cost, and environment friendliness.[13] These properties are especially important for porous mullite, which is used as filter membrane for treatment of great volumes of liquid/gas effluents, which requires the use of porous support with higher porosity and good mechanical strength in order to maintain a lower pressure drop across the filter membrane and to withstand the pressure gradient imposed during practical separation applications.

Traditionally, the open porosity of a ceramic membrane is limited by the intergranular packing effect of the starting powder or precursor, mainly depending on its morphology and particle size distribution. It is well known that porosity can be effectively controlled by varying sintering conditions such as sintering temperature and dwelling time.[14] High temperature partial sintering is required to produce sintering necks, endowing porous ceramic membrane with sufficient strength, while degrading open porosity to some extent. Normally, an improvement in open porosity, which is required to endow a low fluid resistance, is achieved with addition of pore-forming agents such as graphite powder or some organic compounds,[15,16] which burn out or decompose completely during heating. However, the pores produced in this way are usually believed to deteriorate the mechanical reliability.[17] It is usually hard and thus of great importance to find a way to produce high porosity without alteration of mechanical strength of ceramic membrane supports, which are expected to withstand large pressure gradient imposed during practical separation applications. Apart from high mechanical strength, a proper ceramic membrane support should have high permeability.[18]

Recently, mullite whiskers have been widely investigated as candidates for reinforcement of ceramic-based composites due to their high aspect ratio and high strength.[19] Several approaches, such as addition of AlF_3[11,19,20] to starting material mixtures, are developed to produce mullite-whisker-reinforced composites. In order to further enhance mullite phase content at low temperatures, some sintering aids (such as V_2O_5,[21] MgO,[22] TiO_2[12] and WO_3[23]) are used during fabrication of low-cost porous mullite. However, there are few reports with MoO_3 as sintering additive. Since Mo and W are in the same subgroup of the element periodic table, associated with the lower melting point of MoO3 (795 °C), it is expected that addition of MoO_3 accelerates the growth of mullite crystals and thus enhances mullite content at lower temperatures.

Different from traditional particle packing structure processed by partial sintering, in this work, with MoO_3 and AlF_3 as additives, a highly porous structure of inter-locked mullite whiskers is realized in mullite membrane support made from waste coal fly ash and bauxite. The present study aims at elaborating a new type of porous structure for ceramic membrane support with enhanced porosity and permeance, but without significant degradation of mechanical property. The effect of additives and sintering parameters on the main properties of porous mullite membrane supports is studied in detail, mainly including porosity, mechanical properties, pore size distribution, micro-structure (SEM and phase compositions) and permeance.

2. Experimental procedures

2.1. Starting materials for membrane support

Coal fly ash (Ningbo, Zhejiang Province, China) and nature bauxite (Yangquan, Shanxi Province, China) were used as the starting materials. AlF_3 (98–102%, Guangfu Fine Chemical Reagent Ltd., Tianjin, China) and MoO_3 (Sinopharm Chemical Reagent Co., Ltd) were used as crystallization catalyst and mineralizer, respectively.

Based on mullite stoichiometric composition ($3Al_2O_3{\cdot}2SiO_2$), a series of MoO_3–AlF_3 doped and undoped mullite membrane supports were prepared by adding various weight percents (wt.%) of AlF_3 (x wt.%) and MoO_3 (y wt.%) into the powder mixture of fly ash and bauxite. All samples are labeled as AxMy. A stands for AlF_3, M for MoO_3, and the numbers following them represent their mass percentage in the samples (e.g. A0M0 for the sample without addition of AlF_3 and MoO_3, A4M5 for the sample with addition of 4 wt.% of AlF_3 and 5 wt.% of MoO_3).

2.2. Fabrication of membrane support

The raw materials with different compositions were wet-ball-milled in distilled water for 12 h using a planetary ball-milling machine (SFM-1, Hefei Kejing Materials Technology Co., Ltd) at a milling speed of 400 rpm. After complete drying, the milled powders were uniformly mixed with organic binder PVA-1750 (5.0 wt.% solution) in an alumina mortar and then uniaxially pressed into cylindrical pellets (20 mm in diameter and 1–2 mm in thickness) at a pressure of 190 MPa. The green disc-shape membrane supports were placed in a closed alumina crucible and sintered in an electrically heated muffle furnace in air at final temperatures ranging from 1100 °C to 1500 °C for 2 h.

2.3. Characterization and test

Particular emphasis is placed on characterization of membrane properties of the supports: open porosity, pore size distribution, mechanical strength, gas and water permeances. A detailed microstructural analysis was performed to understand the formation process and the reinforcement of this mullite membrane support.

The particle size distribution of fly ash and bauxite was determined by a laser particle size analyzer (Mastersizer 2000, Malvern Instruments Ltd., UK). Chemical compositions of the raw materials (coal fly ash and natural bauxite) were examined by X-ray fluorescence spectrometry (WDXRF, PANalytical Corporation, The Netherlands).

Open porosity was determined by the Archimedes method[24] with water as the liquid medium. Pore size distribution was measured by a pore size distribution analyzer (PSDA-20, Nanjing Gaoqian function materials Co. Ltd., China) based on a gas–liquid displacement method. The pore diameter can be

calculated from the Washburn's equation using the bubble-point method[22,25,26]:

$$d = \frac{4\gamma \cos\theta}{\Delta p} \quad (1)$$

where γ is the surface tension coefficient of the liquid, θ is the contact angle of the liquid on the pore wall and Δp is the applied pressure difference. In most cases, the shape of the pore tunnels is irregular, and the pore size is thus defined as the diameter of a circle which area is equal to the pore throat.[25]

Biaxial flexural strength (BFS) was measured by a universal testing machine (AGS-X, Shimadzu Ltd., Japan). BFS was calculated using the formula for maximum tensile stress given by Timoshenko and Woinowsky-Krieger[27]:

$$\text{BFS (MPa)} = \frac{N}{t^2}\{(1+\nu)[(0.485\ln(a/t)+0.52]+0.48\} \quad (2)$$

where N is the load (N), ν is Poisson's ratio ($\nu = 0.26$ in this study), a is the radius of the support circle (m) and t is the thickness of the specimen (m).

Weibull analysis was conducted on the results of biaxial flexural strength. The Weibull analysis curves[28] were made using $\ln\sigma$ and $\ln\ln[1/(1-P_f)]$ plot as X-axis and Y-axis, respectively, where σ is the biaxial flexural strength, P_f is he fracture probability. The latter P_f is defined by the relation $P_f = i/(N+1)$, where i is the rank in biaxial flexural strength from smallest to largest and N denotes the total number of samples (here $N = 10$ in our study).

The fracture energy was determined using the following equation:

$$E_a = \sum_{i=1}^{N} \frac{E_i}{\pi a^2 t_i} \times \frac{10^{-3}}{N} \quad (3)$$

where E_a is the fracture energy per unit volume, E_i is the fracture energy of sample i, a is the circumcircle radius of the three support balls ($a = 5$ mm in our study), N is the total number of test bodies ($N = 10$ in our study), t_i is the average thickness of sample i.

Microstructures of the sintered samples were analyzed by scanning electron microscopy (SEM, S-4800, Hitachi LTD., Japan). Phase analysis of the raw materials and sintered samples was determined by X-ray diffraction (XRD, D8 advance, Bruker Corporation, Germany). XRD quantitative analysis based on the normalized reference intensity ratio (RIR) method, was adopted to calculate the mullite content in the sintered samples.[29]

2.4. Water flux and permeance study

A home-made dead-end flow setup was used for water permeance studies. The stainless-steel setup mainly consists of a top cylindrical water container and a base plate with a provision to keep a support. The support is rested on a perforated disk (casing) and placed in the bottom compartment. The transmembrane pressure for these experiments was in the range of 0.05–0.3 MPa. The permeate flow rate was recorded at 10 min intervals for 1 h and the measurements were repeated for all the samples.

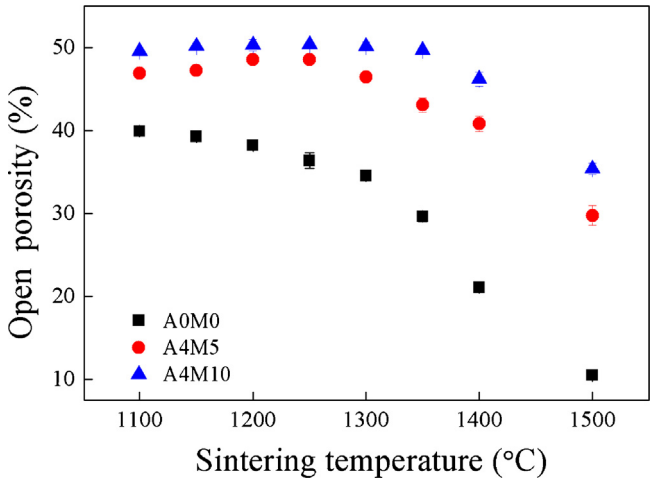

Fig. 1. Open porosities of the sintered membrane supports with addition of 0–10% wt.% of MoO_3 and 0–4% wt.% of AlF_3 as a function of sintering temperature.

2.5. N_2 flux and permeance study

N_2 permeance studies were performed at 25 °C at differential pressures ranging from 0.05 to 0.3 MPa with 0.05 MPa intervals in a dead-end mode with the inlet pressure controlled by a pressure regulator and a digital pressure gauge. The gas flow across the membrane was measured with a bubble flow meter on the exit gas stream of the membrane support. The samples were held at each pressure step until a steady flow rate was achieved.

3. Results and discussion

3.1. Characterization of membrane materials

The chemical compositions of the coal fly ash and bauxite are given in Table 1. The coal fly ash mainly consists of mullite ($3Al_2O_3{\cdot}2SiO_2$, PDF no. 15-0776), belonging to primary mullite, which is formed from aluminosilicate clay minerals during the combustion process of raw coal. As to bauxite, the main crystalline phases detected are diaspore (AlO(OH), PDF no. 87-0705) and kaolinite ($Al_2O_3{\cdot}2SiO_2{\cdot}2H_2O$, PDF no. 78-2109). The average particle diameters of coal flyash and bauxite particles are 2.1 μm and 1.2 μm, respectively. Most of the mixtures particle size after ball-milling center between 1.1 μm (d_{10}) and 4.3 μm (d_{90}) in diameter.

3.2. Open porosity and mechanical property

Fig. 1 indicates that the open porosity without additives (A0M0) shows a gradually-decreasing trend with sintering temperature. This result is similar to porous mullite, derived from the kaoline–alumina system,[30] but different from the trend of increasing porosity with increasing sintering temperature at certain range for the fly-ash–bauxite system involving

Table 1
Main chemical composition (wt.%) of fly ash and natural bauxite measured by semi-quantitative XRF.

Materials	Chemical composition (%)								
	Al_2O_3	SiO_2	CaO	Fe_2O_3	TiO_2	SO_3	K_2O	Na_2O	Others
Fly ash	44.76	44.17	4.57	3.02	1.92	0.44	0.4	0.22	0.49
Bauxite	63.53	10.41	0.47	7.08	2.98	0.18	0.28	0.15	0.52

The loss on ignition of fly ash and bauxite is 1.01 and 14.40 wt.%, respectively.

a sintering self-expansion, as reported in Ref. [6], which is possibly due to the difference in chemical compositions of raw materials. The samples with MoO_3 and AlF_3 (A4M5 and A4M10) have higher porosities at all temperatures as compared with A0M0. For A4M5, porosities as high as 46.9 ± 0.4–$48.6 \pm 0.5\%$ are achieved at 1100–1300 °C, then decreased to 41.6 ± 0.9–$29.8 \pm 1.2\%$ at 1400–1500 °C due to the occurrence of a sintering densification. With addition of the same amount of AlF_3 (4 wt.%), open porosity slightly increases with MoO_3 content (from 5 to 10 wt.%). These results indicate that co-addition of MoO_3 and AlF_3 is quite effective in enhancing open porosity of mullite membrane supports.

When comparing A4M5 with A0M0, it is interesting to note that the increase in porosity of the samples with addition of AlF_3 and MoO_3 is not followed by the degradation in mechanical strength at temperatures below 1300 °C (see Fig. 2a). The biaxial flexural strengths of the A4M5 samples are at the same level with those of the samples without any additive from 1100 °C to 1200 °C. Although the strengths of A4M5 are lower than those of A0M0 at 1300–1500 °C, higher porosity enhancements are realized for A4M5 when compared with A0M0. In particular, given the same level of biaxial flexural strength, A4M5 always exhibits higher porosity than A0M0 (Fig. 2b).

Fracture energy (Fig. 2c) of A4M5 and A0M0 gradually increases with sintering temperature, which is consistent with the variation of biaxial flexural strength with sintering temperature (Fig. 2a). At each temperature, A4M5 exhibits higher fracture energy than A0M0. From 1100 to 1400 °C, the fracture energy of A0M0 increases from 8.7 ± 2.1 to 25.4 ± 2.0 kJ m^{-3}. Upon MoO_3 and AlF_3 addition, the samples exhibit higher fracture energy (9.6 ± 2.1 to 30.0 ± 2.2 kJ m^{-3}). These improvements of fracture energy are ascribed to a new structure of a large quantity of compact interlocked needle-like mullite whiskers, which will be studied by SEM (Fig. 7). This effect is similar to that reported by Li et al.,[21] where microstructural homogeneity was improved and mechanical properties could be tuned by doping with V_2O_5.

Fig. 2d shows the Weibull analysis of the biaxial flexural strength results of A0M0 and A4M5 sintered at 1200–1400 °C. Most of the points ($\ln\sigma$ versus $\ln\ln[1/(1-P_f)]$) center close to the corresponding fit lines, which proves a good reliability of the BFS results.

In summary, with addition of MoO_3 and AlF_3, open porosity is significantly improved without degradation of mechanical strength. At the same level of strength, A4M5 always exhibits higher open porosity than A0M0. The A4M5 membrane support sintered at 1200 °C possesses an enhanced open porosity as high as approximately $48.6 \pm 0.5\%$, and an excellent strength of 81.2 ± 3.2 MPa. For filtration membrane application, pore size distribution, gas and water permeation properties are important and thus studied in the following subsections.

3.3. Pore size distribution

Pore size distributions are closely related to final sintering temperatures. A0M0 shows a unimodel distribution of pore size for all the sintering temperatures. The average pore sizes of A0M0 (Fig. 3a) are found to be 0.32, 0.33 and 0.37 sintered at 1200 °C, 1250 °C, and 1300 °C, respectively. A gradual increase in average pore size is observed due to the sintering-induced growth of grains (which will be justified by the SEM results, Fig. 6), leading to the formation of large pores and elimination of small pores at high temperature. These trends are similar with mullite membrane supports prepared in previous work.[6]

Compared with A0M0, the mean pore sizes of A4M5 become smaller at all sintering temperatures. The average pore diameters at 1200 °C, 1250 °C and 1300 °C are 0.18, 0.15 and 0.26, respectively (Fig. 3b). The membranes supports show typical bimodal pore size distributions having maximum number of pores in two regions, 56–70% of pores between 0.20 and 0.45 μm and 30–44% of pores between 0.08 and 0.20 μm. Based on the SEM images shown in Fig. 7, the bimodal pore size distributions are probably due to the formation and growth of stiff skeleton needle-like mullite crystals, resulting in formation of some finer pores among them.[26]

3.4. XRD analysis

Fig. 4 indicates that the two XRD patterns of A0M0 and A4M5 sintered at 1100 °C are similar, consisting of mullite (PDF no. 15-0776) characteristic peaks, weak characteristic peaks of cristobalite (PDF no. 27-0605) and corundum (PDF no. 10-0173). The dependence of mullite phase content on sintering temperature based on RIR analysis (Fig. 5) shows the mullite content in A0M0 (28%) is lower than that in A4M5 (48%). In the A0M0 sample, cristobalite is detected until 1250 °C, which reacted with alumina, contributing to the formation of mullite phase. While in the A4M5 sample, cristobalite is not detected when the sintering temperature increases up to 1200 °C, where the mullite content is 72%. This great increase in mullite content from 48% to 72% is due to the rapid formation of secondary mullite from 1100 °C to 1200 °C. The content of mullite does not significantly increase between 1200 °C and 1400 °C. By contrast, the content of mullite in A0M0 increases gradually from 32% to 76% as the sintering temperature increases from 1100 °C to 1300 °C.

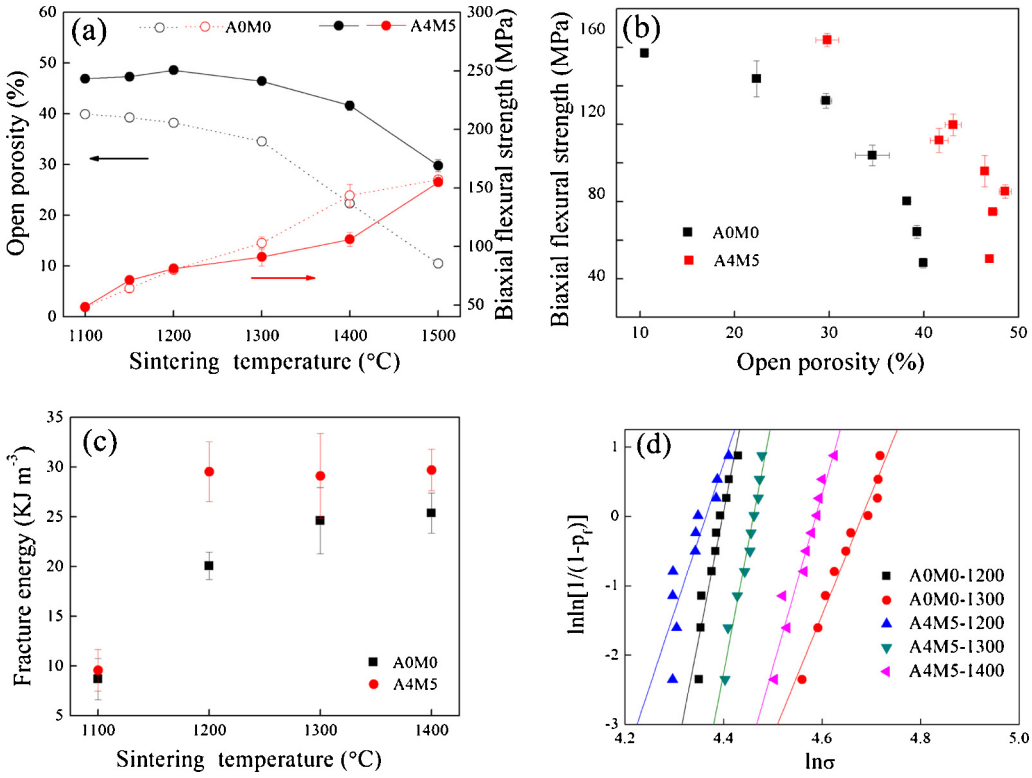

Fig. 2. Biaxial flexural strength test results of the membrane supports with various compositions (a) biaxial flexural strength and open porosity versus sintering temperature, (b) biaxial flexural strength versus porosity, (c) fracture energy versus sintering temperature and (d) Weibull analysis. Standard deviations are not presented as they are very small.

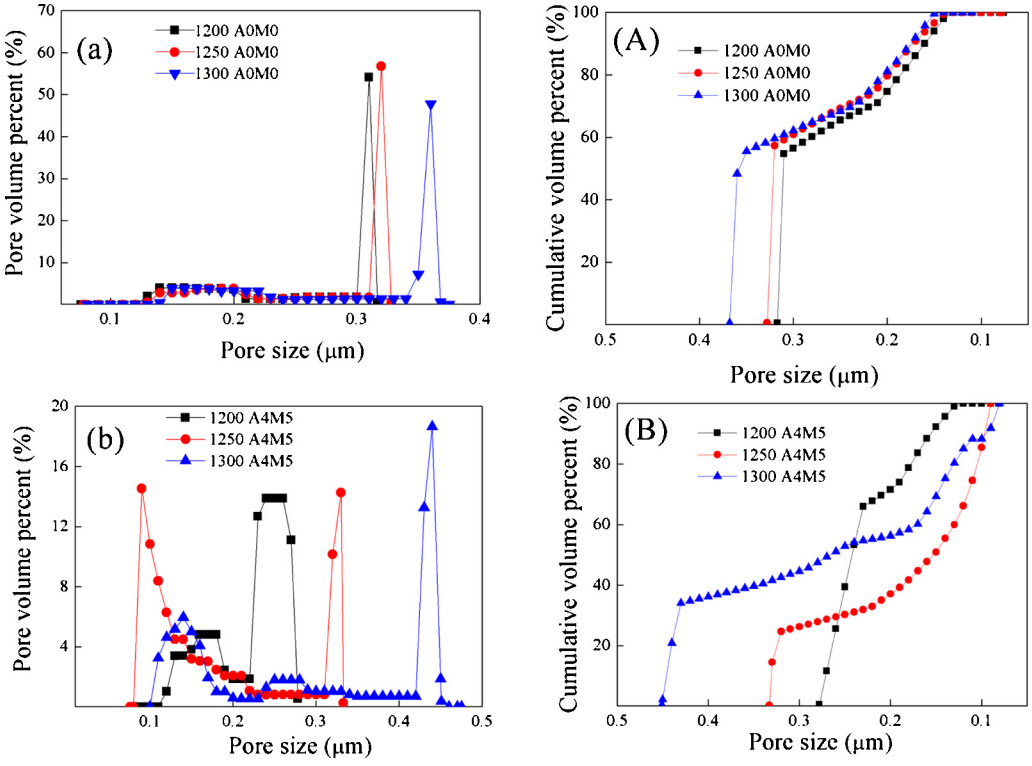

Fig. 3. Pore size distributions of A0M0 ((a) and (A)) and A4M5 ((b) and (B)) sintered at different temperatures.

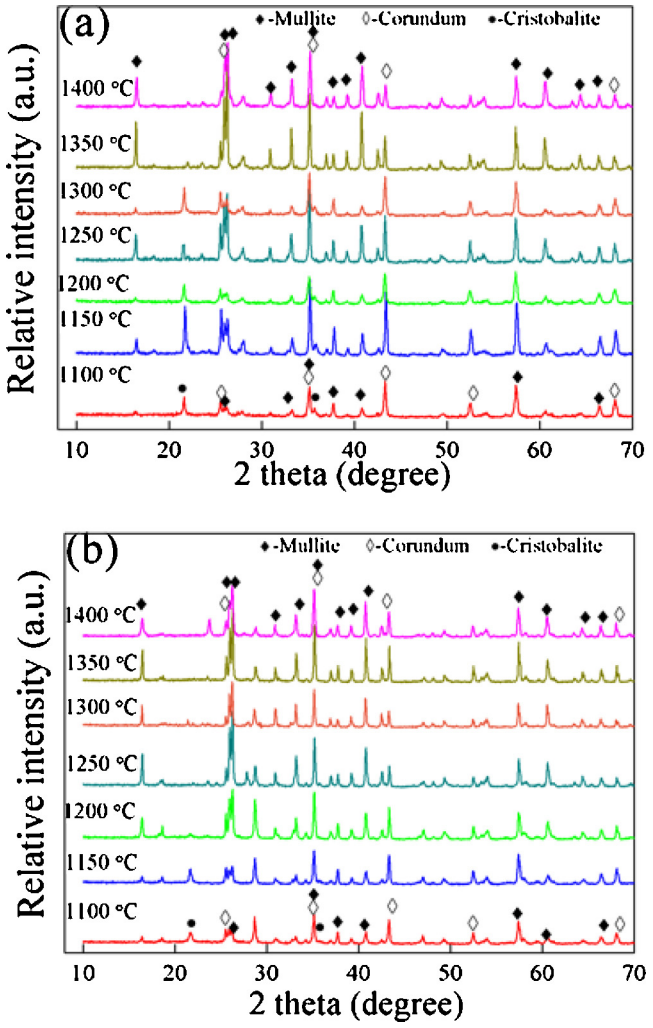

Fig. 4. XRD patterns of the A0M0 (a) and A4M5 (b) membrane supports sintered at various temperatures for 2 h.

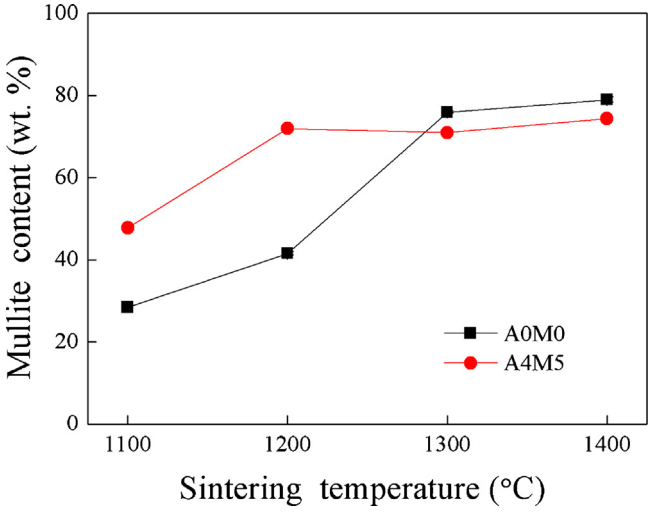

Fig. 5. Effect of sintering temperature on mullite content in the A4M5 and A0M0 membrane supports.

During high-temperature sintering, Firstly, AlF_3 reacted with O_2 to form AlOF, and then AlOF reacted with the reaction product SiF_4 to produce mullite at a lower temperature. The existence of MoO_3 lowered the melting temperature of silica-rich glassy liquid and decreased the high-temperature viscosity of the liquid system, which was favorable to the formation of silica-rich liquid phase and thus promoted mass transportation during the reaction between Al_2O_3 and SiO_2. The Al_2O_3 dissolved into the glassy phase for second mullite formation. While the reaction between Al_2O_3 and SiO_2 went on, the mullite crystals grew up. The excess SiO_2 in fly ash was thus consumed with the rapid formation of large crystals of secondary mullite at 1100–1300 °C. It is reasonable to assume that MoO_3 acted as heterogeneous centers where mullite nucleation could be induced at lower temperatures, leading to lower mullitization temperature. This is similar with the positive effect of V_2O_5 on sintering of mullite membrane supports.[21] With AlF_3 and MoO_3 addition, the temperature, at which mullite phase was formed, is lowered by 150 °C as compared with the samples prepared without any additives.

3.5. Microstructural analysis of membrane support

There is a great difference in microstructure evolution for A0M0 and A4M5 (Figs. 6 and 7). From Fig. 6a, it is found that porous structure is formed by partial-sintering of mixture particles of fly ash and bauxite without morphological change (A0M0) at 1100 °C. From 1200 to 1300 °C (Fig. 6b and c), sintering is gradually enhanced with the presence of larger pores at 1300 °C, which is consistent with the pore size distribution results (see Fig. 3a). With further increasing firing temperature up to 1400 °C, an obvious densification is observed, which corresponds to the rapid decrease in open porosity as discussed above (see Fig. 1).

Comparing Fig. 6a–d with Fig. 7a–d, it is found that with the addition of the additives, a large amount of very fine mullite whiskers are observed to be distributed around some large particles in a porous structure at 1100 °C. With increasing temperature to 1200 °C, a uniform porous microstructure is formed, entirely composed of grown mullite whiskers (Fig. 7b), which act as a skeleton of pore structure. With further increasing sintering temperature (1300 °C) (Fig. 7c), mullite whiskers grow thicker and longer and interlocked with each other. A highly porous structure is observed for the sample sintered at 1300 °C. The formation of stiff skeleton needle-like mullite is very favorable to increase the open porosity (consistent with the above results in Fig. 2). The surface of A4M5-1300 is more porous than that of A0M0-1300, indicating that the accelerated anisotropical growth of mullite whiskers induced by AlF_3 and MoO_3 favors the enhancement of open porosity (consistent with the above results in Fig. 1). This type of grain morphology is quite essential for developing highly porous filtration membrane with strong mechanical integrity.

Fig. 8 shows the freshly fractured surface SEM images, after biaxial flexural strength tests, of A0M0 and A4M5 membrane supports sintered at 1200 °C and the proposed fracture mechanism schematic diagram. For A0M0 sintered at 1200 °C

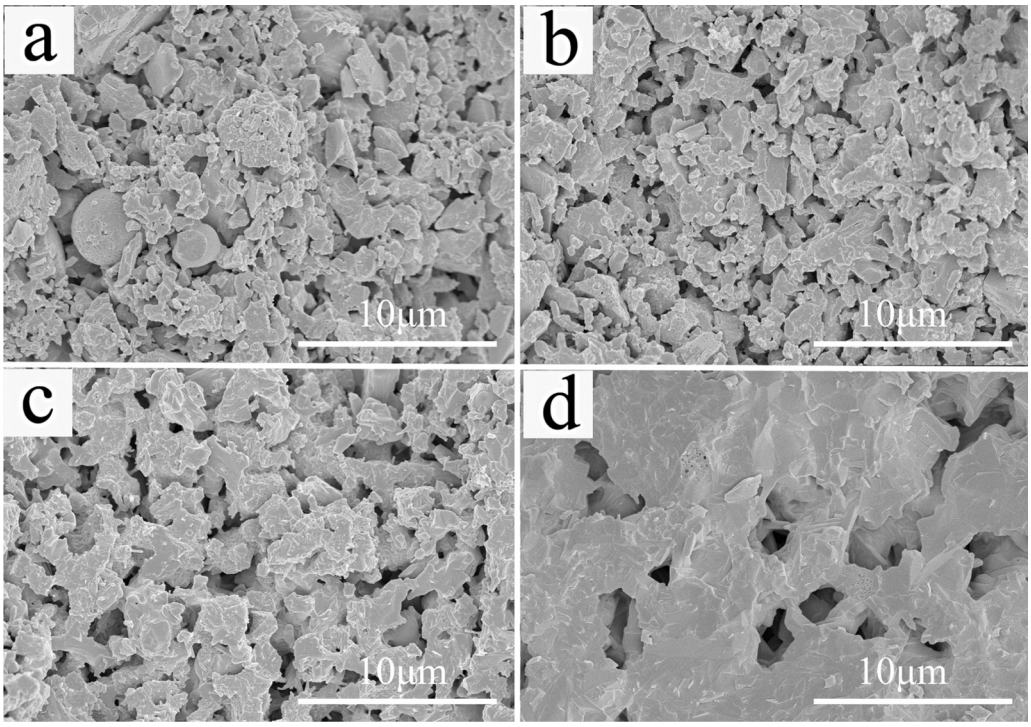

Fig. 6. Fracture surface SEM images of the A0M0 membrane supports sintered at various temperatures: (a) A0M0—1100 °C, (b) A0M0—1200 °C, (c) A0M0—1300 °C and (d) A0M0—1400 °C.

(Fig. 8a), most of the fractures upon failure occur from larger glassy phase regions between partially-sintered mullite crystals (as those indicated by red circles in the fracture mechanism schematic diagram made using CATIA software). The fracture is completely intergranular, which absorbs lower fracture energy during strength test because of lower intrinsic strength of glassy phase (see Fig. 2c). Due to the addition of MoO_3 and AlF_3, open porosity becomes higher, while there is also a significant change in the microstructure of the fabricated mullite membrane support, which is entirely composed of interlocked

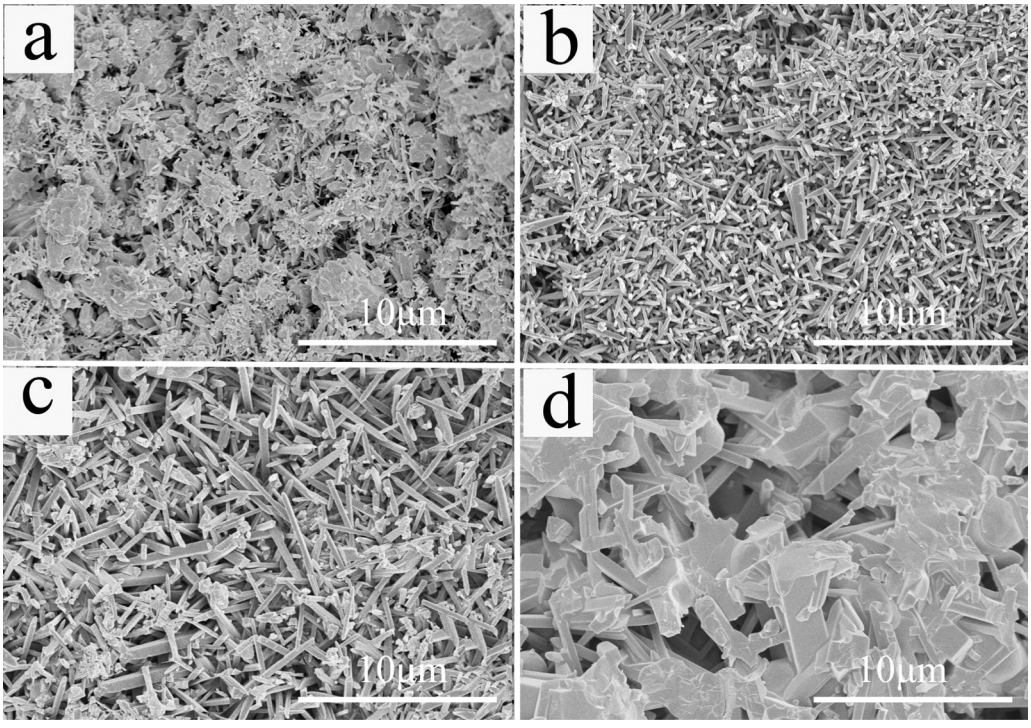

Fig. 7. Fracture surface SEM images of the A4M5 membrane supports sintered at various temperatures: (a) A4M5—1100 °C, (b) A4M5—1200 °C, (c) A4M5—1300 °C and (d) A4M5—1400 °C.

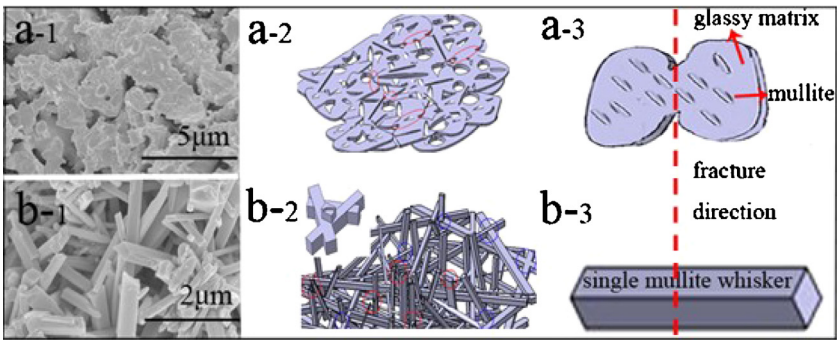

Fig. 8. Freshly fractured surface SEM images (left) and fracture mechanism schematic diagram (right) of the A0M0 (a) and A4M5 (b) membrane supports sintered at 1200 °C after biaxial flexural strength tests.

mullite whiskers without the presence of glassy phase. The intergrown rod-like mullite crystals (as those indicated by the circles in Fig. 8b) could impart good mechanical strength and structure rigidity to the porous mullite support. These inter-locked mullite whiskers are expected to exhibit excellent mechanical properties such as high strength and high modulus since they absorb much higher fracture energies than partially-sintered glassy phase particles (see Fig. 2c), consequently resulting in an enhancement in mechanical strength.[19,22] Possible bridging crack and pull-out of bonded mullite whiskers in aligned way also contribute to this enhancement in strength,[31] as well indicated in Fig. 8b.

In summary, with addition of MoO_3 and AlF_3, formation of more inter-locked mullite whiskers, which adsorb more energy during fracture, is responsible for the improvement in open porosity of A4M5 and mechanical strength compared with A0M0 sintered from 1100 to 1400 °C. Besides, possible bridging crack and pull-out of bonded mullite whiskers in aligned way also contribute to this strength enhancement.

3.6. Water permeance across membrane supports

Water flux (Fig. 9a) of A0M0 and A4M5 increases with transmembrane pressure as well as sintering temperature. In all cases, the water flux increases linearly with transmembrane pressure, which indicates that pressure difference is the only driving force for the permeation of water. When the transport mechanism follows the viscous flow model, the flux versus transmembrane pressure plot should be expressed as a straight line which coincides with the origin (Darcy's law),[32] as indicated in this study. Similar trends were also reported for the other porous inorganic clay-based membranes.[5] In Fig. 9b, an approximately linear relationship exists between water permeance and average transmembrane pressure, indicating a preferential laminar flow mechanism in the mullite membrane supports.[33]

3.7. Nitrogen gas permeance across membrane supports

A pure, non-adsorbing gas flow through a homogeneous porous structure may be described by Knudsen diffusion, viscous flow, surface diffusion, dissolution diffusion, or some combination of these processes. The mechanism of gas transport through microporous membrane depends upon the pore size (r) of the membrane relative to the mean free path (λ) of the gas molecule. Knudsen diffusion occurs in small pores where collisions of the gas molecules with the pore walls have a significant effect on their movement. Viscous flow describes the situation where the pores are large enough so that the viscosity of the gas controls the flow rate through a porous body. In some cases, permeation may also be enhanced by the reaction of the gas with the pore wall surface, i.e. surface diffusion.

When the membrane has pores comparable to the size to the mean free path of the gas molecule, the permeation flux through the membrane can be considered as a combination of Knudsen diffusion and viscous flow. So the permeation of the gas through the porous structure may be modelled by treating Knudsen diffusion and viscous flow as parallel processes, as shown in the following equation[34]

$$J = \frac{\varepsilon r}{\tau_k\,[2\nu/3RTL]\,P} + \frac{\varepsilon r^2}{\tau_v\,[1/8RTL\eta]\,\bar{p}P} \tag{5}$$

where the flux J of a gas component is a function of: (i) gas properties, such as the gas mean molecular velocity ν of the gas and the viscosity of the gas η, and the gas mean molecular velocity ν is given by

$$\nu = \sqrt{\frac{8RT}{\pi M}} \tag{6}$$

where M is the gas molecular mass; (ii) the differential pressure across the membrane P; (iii) the average pressure within the membrane $\bar{p}$; (iv) the membrane thickness L; and (v) the pore characteristics: open porosity ε, pore radius r and the tortuosity factor of the pores corresponding to either the Knudsen τ_k or viscous flow τ_v mechanisms. The tortuosity factors compensate for the pore structure features, which deviate from uniform straight pore structure. The gas permeance of a porous membrane, which is equal to the flux normalized by the pressure difference of the gas across the membrane (J/P), is given by

$$\frac{J}{P} = \frac{\varepsilon r}{\tau_k\,[2\nu/3RTL]} + \frac{\varepsilon r^2}{\tau_v\,[1/8RTL\eta]\,\bar{p}} \tag{7}$$

Plotting the gas permeance vs. average pressure yields a straight line of the form:

$$\frac{J}{P} = a + b\bar{p} \tag{8}$$

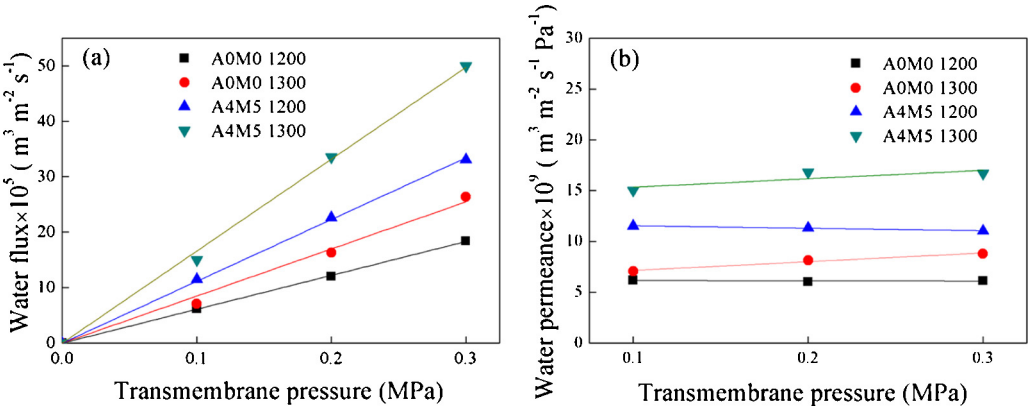

Fig. 9. Water flux (a) and water permeance (b) across the A0M0 and A4M5 membrane supports at several transmembrane pressures.

where the slope a and intercept b are

$$a = F_k = \frac{\varepsilon r}{\tau_k\,[2v/3RTL]} \tag{9}$$

$$b = F_v = \frac{\varepsilon r^2}{\tau_v\,[1/8RTL\eta]} \tag{10}$$

a and b are related to the resistances caused by Knudsen diffusion and viscous flow, respectively.

The permeability in the Knudsen mechanism is constant (independent of transmembrane pressure) and may be related to the porous structure characteristics as described by Eq. (9). At high pressures, the curve keeps as a straight line. The latter section is a pure viscous flow mechanism.[34] This is shown to be the case for nitrogen permeance through the membrane supports, as shown in Fig. 10. The mean pore radius can be determined from the slope and intercept assuming that $\tau_k = \tau_v$[35]:

$$r = \frac{16\eta}{3\,(b/a)\,\sqrt{8RT/\pi M}} \tag{11}$$

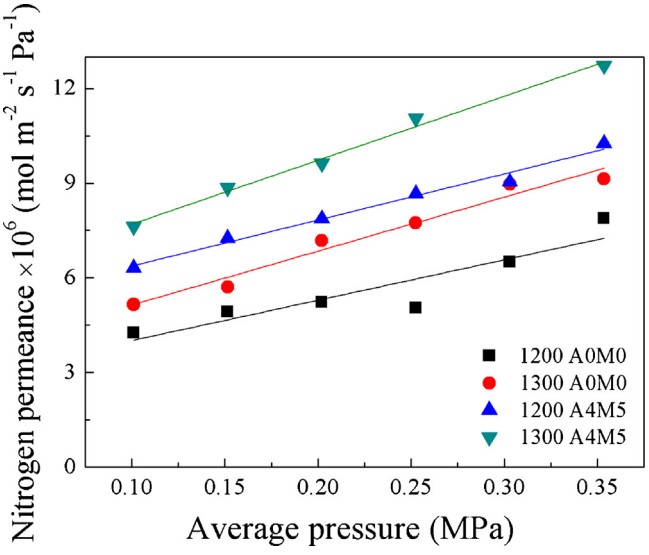

Fig. 10. Nitrogen permeance versus average pressure in the pores of A0M0 and A4M5 membrane supports.

This value of r can then be back substituted into Eq. (7) to obtain the values for tortuosity factors.

The structural parameters and the resulting values of τ, r_C (The mean pore radius calculated from the Knudsen and viscous resistance) of the membrane supports along with the measured mean pore size values (r_M: The mean pore radius measured based on gas-liquid displacement method) for comparison are summarized in Table 2. From Table 2, it can be seen that the values of the mean pore radius r_C obtained from the Knudsen and viscous resistance characteristics are smaller than the results obtained via the gas–liquid displacement method (see Fig. 3). However, the most important concern of gas permeance data is to judge what percentage of the transmembrane flux can be accounted to Knudsen diffusion and viscous flow effects. Table 2 infers that for the membrane supports sintered at 1200–1300 °C, viscous flow contributes to 52–66% of the total flux, conveying that about 52 to 66% of the pores in the membrane supports are well above the range where Knudsen diffusion dominates (1 to 20 nm). This percentage is a little lower than that (70–81%) of the membrane prepared with kaolin.[36] There was a considerable variation in the estimated values of τ for the samples with two different structures. The obtained results suggest that the A0M0 membrane supports have tortuosity values of 2.67 and 2.33 at 1200 and 1300 °C, respectively. Similar results are also found for zirconia and alumina membrane supports.[34,37] With addition of 4 wt.% of AlF_3 and 5 wt.% of MoO_3, the τ decreases down to 1.16 and 1.05, respectively.

Given the same level of biaxial flexural strength, A4M5 membrane supports always exhibit higher nitrogen gas permeance (Fig. 11) than A0M0 at the same temperatures (1100–1500 °C) despite their smaller mean pore size. As verified, introduction of AlF_3 and MoO_3 changes the microstructure with increasing sintering temperature. With addition of 4 wt.% AlF_3 and 5 wt.% MoO_3, since mean pore size decreases a little but porosity increases and tortuosity decreases.

This improvement in gas permeance can be ascribed to a microstructural change of A4M5, featuring a new structure for porous ceramic membrane. The A4M5 samples exhibit a large number of open pores constructed by mullite whiskers with a specific morphology, which are believed to be responsible for accelerating gas flow through the membrane, due to a

Table 2
Characteristics of the A0M0 and A4M5 membrane supports.

Samples	ε	r_M (μm)	r_C (μm)	F_k (%)	F_v (%)	τ
1200-A0M0	0.38	0.32	0.22	36%	64%	2.67
1300-A0M0	0.35	0.37	0.25	34%	66%	2.33
1200-A4M5	0.49	0.18	0.13	48%	52%	1.16
1300-A4M5	0.46	0.26	0.21	44%	56%	1.05

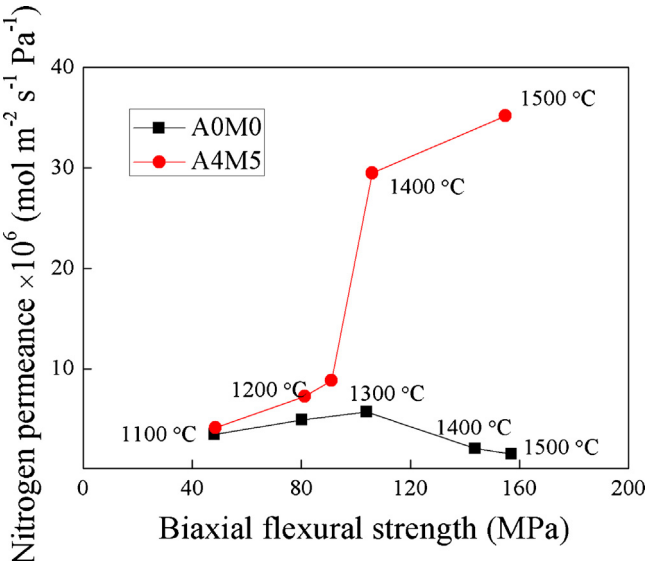

Fig. 11. Nitrogen permeance (at 25 °C and 0.1 MPa) across the A0M0 and A4M5 membrane supports sintered at 1100–1500 °C as a function of average biaxial flexural strength.

lower tortuosity factor (Table 2). A0M0 shows a lower porosity with a microstructure of worse interconnectivity and, therefore, exhibits lower N_2 permeance compared to A4M5, which is consistent with its higher estimated values of τ. Therefore it is concluded that higher permeances of A4M5 are due to higher open porosity and less tortuous paths along the pores, which are produced due to the formation of whisker-structured mullite. Higher permeance with smaller mean pore diameter was also reported in Falamaki's work,[38] where they demonstrated that such an enhancement in permeance was not due to a pore growth mechanism, but to a tortuosity decrease, which was owing to a "round pore shaping" mechanism induced during a liquid-phase sintering process.

4. Conclusions

A ceramic membrane support with increased open porosity and high gas and water permeances, without strength degradation, is prepared from waste fly ash and bauxite, with AlF_3 and MoO_3 as additives. During the sintering, both pore structure and stiff skeleton needle-like structured mullite whiskers were in situ formed, which produced excellent properties including porosity, strength and permeance. The membrane support with 4 wt.% AlF_3 and 5 wt.% MoO_3 (A4M5) exhibits an open porosity as high as 48.6 ± 0.5%, a mechanical strength of 81.2 ± 3.2 MPa, at a lowered sintering temperature of 1200 °C. Also phase formation temperature of mullite membrane supports decreases with addition of AlF_3 and MoO_3. Formation of a porous interlocked and bridging structure with mullite whiskers contributes to the enhancement in open porosity and strength of A4M5 membrane support. In particular, at the same level of strength, A4M5 always shows higher open porosity than A0M0. For this new porous structure ceramic membrane support composed of elongated mullite whiskers, nitrogen gas and water permeances are also enhanced due to a decrease in tortuosity.

Acknowledgements

This work was financially supported by the National Natural Science Foundation of China (no. 21301171 and no. 21376102), the Natural Science Foundation of Fujian Province, China (no. 2014J01215), Ningbo Natural Science Foundation, China (no. 2014A610004), and the Natural Science Foundation of Guangdong Province, China (no. S2013010012199).

References

1. Yoshino Y, Suzuki Y, Nair T, Taguchi BN, Itoh HN. Development of tubular substrates, silica based membranes and membrane modules for hydrogenseparation at high temperature. *J Membr Sci* 2005;**267**:8–17.
2. Van Gestel T, Sebold D, Kruidhof H, Bouwmeester HJ. ZrO_2 and TiO_2 membranes for nanofiltration and pervaporation: Part 2. Development of ZrO_2 and TiO_2 toplayers for pervaporation. *J Membr Sci* 2008;**318**:413–21.
3. DeFriend KA, Wiesner MR, Barron AR. Alumina and aluminate ultrafiltration membranes derived from alumina nanoparticles. *J Membr Sci* 2003;**224**:11–28.
4. Masmoudi S, Ben Amar R, Larbot A, El Feki H, Salah AB, Cot L. Elaboration of inorganic microfiltration membranes with hydroxyapatite applied to the treatment of wastewater from sea product industry. *J Membr Sci* 2005;**247**:1–9.
5. Vasanth D, Pugazhenthi G, Uppaluri R. Fabrication and properties of low cost ceramic microfiltration membranes for separation of oil and bacteria from its solution. *J Membr Sci* 2011;**379**:154–63.
6. Dong Y, Zhou J-E, Lin B, Wang Y, Wang S, Miao L, et al. Reaction-sintered porous mineral-based mullite ceramic membrane supports made from recycled materials. *J Hazard Mater* 2009;**172**:180–6.
7. Weir M, Rutinduka E, Detellier C, Feng C, Wang Q, Matsuura T, et al. Fabrication, characterization and preliminary testing of all-inorganic ultrafiltration membranes composed entirely of a naturally occurring sepiolite clay mineral. *J Membr Sci* 2001;**182**:41–50.
8. Jedidi I, Saïdi S, Khemakhem S, Larbot A, Elloumi -Ammar N, Fourati A, et al. Elaboration of new ceramic microfiltration membranes from mineral coal fly ash applied to waste water treatment. *J Hazard Mater* 2009;**172**:152–8.
9. Blissett R, Rowson N. A review of the multi-component utilisation of coal fly ash. *Fuel* 2012;**97**:1–23.
10. Jung J, Park H, Stevens R. Mullite ceramics derived from coal fly ash. *J Mater Sci Lett* 2001;**20**:1089–91.

11. Li S, Du H, Guo A, Xu H, Yang D. Preparation of self-reinforcement of porous mullite ceramics through in situ synthesis of mullite whisker in flyash body. *Ceram Int* 2012;**38**:1027–32.
12. Dong Y, Hampshire S, Zhou J-e Lin B, Ji Z, Zhang X, et al. Recycling of fly ash for preparing porous mullite membrane supports with titania addition. *J Hazard Mater* 2010;**180**:173–80.
13. Schneider H, Schreuer J, Hildmann B. Structure and properties of mullite—a review. *J Eur Ceram Soc* 2008;**28**:329–44.
14. She J, Ohji T. Fabrication and characterization of highly porous mullite ceramics. *Mater Chem Phys* 2003;**80**:610–4.
15. Mueller J, Cen Y, Davis RH. Crossflow microfiltration of oily water. *J Membr Sci* 1997;**129**:221–35.
16. Studart AR, Gonzenbach UT, Tervoort E, Gauckler LJ. Processing routes to macroporous ceramics: a review. *J Am Ceram Soc* 2006;**89**: 1771–89.
17. Ohji T, Fukushima M. Macro-porous ceramics: processing and properties. *Int Mater Rev* 2012;**57**:115–31.
18. Maarten Biesheuvel P, Verweij H. Design of ceramic membrane supports: permeability, tensile strength and stress. *J Membr Sci* 1999;**156**: 141–52.
19. Peng P, Sorrell C. Preparation of mullite whiskers from topaz decomposition. *Mater Lett* 2004;**58**:1288–91.
20. Okada K, Otuska N. Synthesis of mullite whiskers and their application in composites. *J Am Ceram Soc* 1991;**74**:2414–8.
21. Li J-H, Ma H-W, Huang W-H. Effect of V_2O_5 on the properties of mullite ceramics synthesized from high-aluminum fly ash and bauxite. *J Hazard Mater* 2009;**166**:1535–9.
22. Dong Y, Hampshire S, Zhou J-e, Ji Z, Wang J, Meng G. Sintering and characterization of flyash-based mullite with MgO addition. *J Eur Ceram Soc* 2011;**31**(5):687–95.
23. Kong LB, Huang H, Zhang TS, Ma J, Boey F, Zhang RF, et al. Growth of mullite whiskers in mechanochemically activated oxides doped with WO_3. *J Eur Ceram Soc* 2003;**23**:2257–64.
24. ASTM standard C20-00. *Standard Test Methods for Apparent Porosity, Water Absorption, Apparent Specific Gravity, and Bulk Density of Burned Refractory Brick and Shapes by Boiling Water*. West Conshohocken, PA: ASTM International; 2010.
25. Yu J, Hu X, Huang Y. A modification of the bubble-point method to determine the pore-mouth size distribution of porous materials. *Sep Purif Technol* 2010;**70**:314–9.
26. Chen G, Qi H, Xing W, Xu N. Direct preparation of macroporous mullite supports for membranes by in situ reaction sintering. *J Membr Sci* 2008;**318**:38–44.
27. Timoshenko S, Woinowsky-Krieger S, Woinowsky S. *Theory of plates and shells*. New York, NY: McGraw-Hill; 1959. p. 87–121.
28. Wachtman JB, Cannon WR, Matthewson MJ. *Mechanical properties of ceramics*. New York, NY: Wiley Interscience; 2009.
29. Chung FH. Quantitative interpretation of X-ray diffraction patterns of mixtures. II. Adiabatic principle of X-ray diffraction analysis of mixtures. *J Appl Crystallogr* 1974;**7**:526–31.
30. Donelson R, Paul G, Ciacchi F, Badwal S. Permeation and strength characteristics of macroporous supports for gas separation produced by co-sintering mixtures of α-alumina and kaolin. *J Membr Sci* 2014;**463**:126–33.
31. Ohji T. Microstructural design and mechanical properties of porous silicon nitride ceramics. *Mat Sci Eng A—Struct* 2008;**498**:5–11.
32. Monash P, Pugazhenthi G. Development of ceramic supports derived from low-cost raw materials for membrane applications and its optimization based on sintering temperature. *Int J Appl Ceram Technol* 2011;**8**:227–38.
33. Dong Y, Liu X, Ma Q, Meng G. Preparation of cordierite-based porous ceramic micro-filtration membranes using waste fly ash as the main raw materials. *J Membr Sci* 2006;**285**:173–81.
34. Falamaki C, Afarani MS, Aghaie A. Initial sintering stage pore growth mechanism applied to the manufacture of ceramic membrane supports. *J Eur Ceram Soc* 2004;**24**:2285–92.
35. Meixner DL, Dyer PN. Characterization of the transport properties of microporous inorganic membranes. *J Membr Sci* 1998;**140**:81–95.
36. Nandi B, Uppaluri R, Purkait M. Preparation and characterization of low cost ceramic membranes for micro-filtration applications. *Appl Clay Sci* 2008;**42**:102–10.
37. Wang P, Huang P, Xu N, Shi J, Lin Y. Effects of sintering on properties of alumina microfiltration membranes. *J Membr Sci* 1999;**155**:309–14.
38. Falamaki C, Naimi M, Aghaie A. Dual behavior of $CaCO_3$ as a porosifier and sintering aid in the manufacture of alumina membrane/catalyst supports. *J Eur Ceram Soc* 2004;**24**:3195–201.